DRAFT VERSION OCTOBER 27, 2026
Typeset using LaTeX **twocolumn** style in AASTeX7.0.1

arXiv:2610.33155v1 [astro-ph.GA] 23 Oct 2026

El Ascua: An ultra-luminous, radio-loud, Compton-thick AGN at $z \sim 3.8$ hiding in plain sight revealed by MINERVA multi-band MIRI observations

AIDAN P. CLOONAN [1,*] EDGAR P. VIDAL [2] ALEXANDRA POPE [1] ANNA SAJINA [2,3] NICHOLAS S. MARTIS [4]
YOSHIHISA ASADA [3,5,†] OLIVIA R. COOPER [6,‡] ADAM MUZZIN [7] STACEY ALBERTS [8]
JACQUELINE ANTWI-DANSO [3,1,§] GABRIEL BRAMMER [9,10] SAM E. CUTLER [2] KARTHEIK G. IYER [11,¶] IVO LABBÉ [12]
DANILO MARCHESINI [2] TIM B. MILLER [13] IKKI MITSUHASHI [6] LUKE ROBBINS [2] GHASSAN T. E. SARROUH [7]
MONU SHARMA [14] MAURO STEFANON [14,15] KATHERINE A. SUESS [6] KATHERINE E. WHITAKER [1,9]
CHRIS J. WILLOTT [16] PRATIKA DAYAL [17,3,18] ANNA DE GRAAFF [19] BEN FORREST [6] KARL GLAZEBROOK [12]
JENNY E. GREENE [20] KELSEY HARGRAVES [21] WILLIAM W.H. JARVIS [1] DANIEL J. LYON [12] IAN MCCONACHIE [22]
GAËL NOIROT,[23] VERONICA PRATT [2] AND BINGJIE WANG [20,¶]

[1] *Department of Astronomy, University of Massachusetts, Amherst, MA 01003, USA*
[2] *Department of Physics and Astronomy, Tufts University, 574 Boston Avenue, Suite 304, Medford, MA 02155, USA*
[3] *David A. Dunlap Department of Astronomy & Astrophysics, University of Toronto, 50 St. George Street, Toronto, ON M5S 3H4, Canada*
[4] *University of Ljubljana, Faculty of Mathematics and Physics, Jadranska ulica 19, SI-1000 Ljubljana, Slovenia*
[5] *Waseda Research Institute for Science and Engineering, Faculty of Science and Engineering, Waseda University, 3-4-1 Okubo, Shinjuku, Tokyo 169-8555, Japan*
[6] *Department for Astrophysical & Planetary Science, University of Colorado, Boulder, CO 80309, USA*
[7] *Department of Physics and Astronomy, York University, 4700 Keele St., Toronto, Ontario, M3J 1P3, Canada*
[8] *AURA for the European Space Agency (ESA), Space Telescope Science Institute, 3700 San Martin Dr., Baltimore, MD 21218, USA*
[9] *Cosmic Dawn Center (DAWN), Copenhagen, Denmark*
[10] *Niels Bohr Institute, University of Copenhagen, Jagtvej 128, DK-2200 Copenhagen N, Denmark*
[11] *Columbia Astrophysics Laboratory, Columbia University, 550 West 120th Street, New York, NY 10027, USA*
[12] *Centre for Astrophysics and Supercomputing, Swinburne University of Technology, Melbourne, VIC 3122, Australia*
[13] *Center for Interdisciplinary Exploration and Research in Astrophysics (CIERA), Northwestern University, 1800 Sherman Ave, Evanston, IL 60201, USA*
[14] *Departament d'Astronomia i Astrofisica, Universitat de Valencia, C. Dr. Moliner 50, E-46100 Burjassot, Valencia, Spain*
[15] *Unidad Asociada CSIC "Grupo de Astrofisica Extragalactica y Cosmologi" (Instituto de Fisica de Cantabria - Universitat de Valencia)*
[16] *National Research Council of Canada, Herzberg Astronomy & Astrophysics Research Centre, 5071 West Saanich Road, Victoria, BC, V9E 2E7, Canada*
[17] *Canadian Institute for Theoretical Astrophysics, 60 St George St, University of Toronto, Toronto, ON M5S 3H8, Canada*
[18] *Department of Physics, 60 St. George Street, University of Toronto, Toronto, ON M5S 3H8, Canada*
[19] *Max-Planck-Institut für Astronomie, Königstuhl 17, D-69117, Heidelberg, Germany*
[20] *Department of Astrophysical Sciences, Princeton University, 4 Ivy Lane, Princeton, NJ 08544, USA*
[21] *School of Chemistry and Physics, 2 George St, Queensland University of Technology, Brisbane, QLD 4000, Australia*
[22] *Department of Astronomy, University of Wisconsin-Madison, 475 N. Charter St., Madison, WI 53706 USA*
[23] *Space Telescope Science Institute, 3700 San Martin Drive, Baltimore, MD 21218, USA*

(Received XXX; Revised XXX; Accepted XXX)

Submitted to ApJL

ABSTRACT

Heavily dust-obscured active galactic nuclei (AGN) are crucial for understanding supermassive black hole growth. Using multi-band MIRI photometry from the MINERVA survey, we report the discovery in the UDS field of an extremely mid-infrared bright Compton-thick AGN (CT AGN) at $z \sim 3.8$, *el Ascua* (the Ember). The AGN and/or its host galaxy is detected at 870 μm with ALMA and at 1.4 GHz with the VLA. With UV-to-radio spectral energy distribution modeling, we estimate that the dusty host galaxy has a stellar mass of $\log\left(M_\star/M_\odot\right) = 10.82 \pm 0.57$ and a star formation rate of SFR $= 157 \pm 8\, M_\odot \mathrm{yr}^{-1}$, and we confirm the presence of a powerful dusty AGN with an intrinsic accretion luminosity of $\log\left(L_{\mathrm{acc}}/\mathrm{erg\ s}^{-1}\right) = 47.12 \pm 0.58$. CT obscuration is revealed by comparing the upper limit on the X-ray luminosity over $2-10$ keV with the 6 μm mid-IR AGN luminosity. We additionally find evidence for a radio excess by comparing its total IR-to-radio ratio to those of typical star-forming galaxies and radio-quiet AGN, implying that *el Ascua* could be a rare radio-loud

Email: apcloonan@umass.edu

CT AGN. With an extremely high ratio between black hole accretion rate and SFR, the AGN is likely nearing the peak of a deeply obscured phase of black hole growth before AGN feedback blows away the obscuring material. Our work demonstrates the power of MIRI to reveal heavily obscured AGN missing from our supermassive black hole census.

Keywords: Active galactic nuclei (16) — Galaxy evolution (594) — Infrared galaxies (790) — Supermassive black holes (1663) — AGN host galaxies (2017)

1. INTRODUCTION

Most active galactic nuclei (AGN) are obscured by interstellar gas and dust (e.g., R. C. Hickox & D. M. Alexander 2018), and at $z > 0$ these obscured AGN are the dominant mode for the growth of supermassive black holes (SMBHs; e.g., G. Yang et al. 2023; T.-E. Bulichi et al. 2026). In particular, Compton-thick AGN (CT AGN), with gas column densities of $N_H \gtrsim 1.5 \times 10^{24}\,\mathrm{cm}^{-2}$ attenuating soft X-ray emission (i.e., of energy < 10 keV) from hot coronal gas near the accretion disk, are required to match the cosmic X-ray background (e.g., R. Gilli et al. 2007; A. R. Draper & D. R. Ballantyne 2010). CT AGN make up a significant fraction of AGN at $z = 0$, though the exact number is uncertain with estimates ranging from $\sim 20\%$ to $\sim 50\%$ of AGN (D. Burlon et al. 2011; M. Brightman & Y. Ueda 2012; G. Lanzuisi et al. 2018; T. T. Ananna et al. 2019). In the local universe, CT AGN can be found in the heavily buried nuclei of luminous and ultra-luminous infrared galaxies (LIRGs/ULIRGs), with $\sim 20-40\%$ of nearby ULIRGs hosting CT AGN (e.g., E. Nardini & G. Risaliti 2011; F. E. Bauer et al. 2015; S. Yamada et al. 2020; N. Falstad et al. 2021; M. A. Johnstone et al. 2025). At $z \gtrsim 1$, CT AGN account for anywhere from $\sim 33\%$ to $> 50\%$ of AGN (e.g., F. E. Bauer et al. 2010; M. Brightman & Y. Ueda 2012; J. Buchner et al. 2015; A. Del Moro et al. 2016; G. Lanzuisi et al. 2018; M. Lacy & A. Sajina 2020; C. M. Carroll et al. 2023), meaning that a similar or even higher fraction of AGN are CT in the distant universe compared to $z = 0$ (E. Treister et al. 2009). CT AGN consequently reflect a key evolutionary phase in SMBH growth, and studying their accretion properties, interstellar environments, and host galaxies is critical for comprehensive models of black hole growth, obscuration, fueling, and feedback.

CT AGN are notoriously difficult to identify and confirm beyond the local universe, as the observed X-ray luminosity at < 10 keV is tens or hundreds of times fainter than the intrinsic, unabsorbed value (A. Comastri 2004). Furthermore, X-ray surveys are not sufficiently deep at harder rest-frame X-ray energies of > 10 keV where the obscuring material is more optically thin (R. Gilli et al. 2007). As a result, a significant number of distant CT AGN are missed by both soft and hard X-ray surveys.

Infrared (IR) observations are therefore crucial for identifying and characterizing CT AGN (J. Lyu & G. Rieke 2022; A. Sajina et al. 2022), especially at $z > 0$ where X-ray constraints are normally unavailable (R. Gilli et al. 2014; F. Vito et al. 2020). In lieu of X-ray detections, studies of CT AGN have often paired the weak or non-detected X-ray flux with spectral features in the rest-frame mid-IR (MIR) at $3-30\,\mu$m (e.g, E. Daddi et al. 2007; D. M. Alexander et al. 2008; F. Fiore et al. 2009; P. Gandhi et al. 2009; A. D. Goulding et al. 2012; R. Gilli et al. 2014; G. B. Lansbury et al. 2015; J. Lyu et al. 2024; X. Guo et al. 2025), where the MIR flux density from an AGN originates from a warm dusty torus enveloping the SMBH and the accretion disk (e.g., R. C. Hickox & D. M. Alexander 2018; J. Lyu & G. Rieke 2022). The MIR features often associated with AGN include the continuum from the warm dusty torus which brightens towards redder MIR wavelengths, forbidden emission lines from ions requiring high ionization potential, and broad absorption features at $9.7\,\mu$m and $18\,\mu$m from silicate dust grains in the foreground of the warm dust continuum (A. Sajina et al. 2022). Spectral energy distribution (SED) modeling has allowed for disentangling the AGN warm dust from polycyclic aromatic hydrocarbons (PAHs; A. Pope et al. 2008; A. Kirkpatrick et al. 2012, 2015). PAHs trace star formation and the interstellar medium, and they exhibit unique spectral features in the mid-IR, whereas the warm dusty torus of an AGN shows a strong, red, power-law continuum which can outshine the PAHs. The shape of the mid-IR SED therefore is sensitive to the relative contributions of PAHs and dusty torus emission. However, at $z \gtrsim 1$ studies with *Spitzer* and *Herschel* are generally limited to the brightest obscured AGN (e.g., M. Lacy et al. 2007; D. M. Alexander et al. 2008; F. E. Bauer et al. 2010; C. Gruppioni et al. 2013; C. M. Carroll et al. 2023), rendering larger statistical samples of distant obscured AGN difficult to compile.

The first several years of *JWST* results, especially with the Mid-IR Instrument (MIRI), have dramatically changed the broader landscape of obscured AGN science. The large increase in sensitivity that MIRI provides is pushing population studies of dusty galaxies and AGN to cosmic noon ($z \sim 2$)

* NSF Graduate Research Fellow
† Dunlap Fellow
‡ NSF Astronomy and Astrophysics Postdoctoral Fellow
§ Banting Postdoctoral Fellow
¶ NHFP Hubble Fellow

and beyond (e.g., A. Kirkpatrick et al. 2023; S. Alberts et al. 2024; B. E. Backhaus et al. 2026). With up to eight broad-band filters spanning $5-25\,\mu$m, the photometric sampling of the SED allows for more robust decomposition of AGN and PAH emission (G. Yang et al. 2023; J. Lyu et al. 2024; T.-E. Bulichi et al. 2026), giving stronger constraints on AGN activity across the whole luminosity function. J. Lyu et al. (2024) demonstrate these improvements for CT AGN as part of a broader overview of the power MIRI provides for finding more complete obscured AGN samples. Even without MIRI, R. Maiolino et al. (2025) measure AGN bolometric luminosities from *JWST* near-IR spectra and combine with X-ray brightness to find heavily obscured AGN at $z > 4$, where MIRI no longer probes the rest-frame mid-IR. Between *JWST*'s IR capabilities and archival X-ray data, we can now reliably find CT AGN beyond the local universe without relying on rare X-ray detections.

In this *Letter*, we report the discovery of an extremely luminous CT AGN at $z_{\rm phot} \approx 3.77$ in the Ultra-Deep Survey (UDS) extragalactic field (A. Lawrence et al. 2007) with the "Medium-band Imaging with NIRCam to Explore ReVolutionary Astrophysics" (MINERVA) program (GO-7814, PIs: Muzzin, Suess, Marchesini; A. Muzzin et al. 2025). The CT AGN, located at J021725−051427, is associated with a sub-millimeter galaxy (SMG) with a strong Band 7 detection in archival ALMA imaging. While it has been flagged previously as a radio source (C. Simpson et al. 2006; B. Zhang et al. 2025), its obscured AGN activity—much less its CT nature—has not been previously explored. We briefly describe how the source was identified, and we combine the *JWST* data with archival X-ray, optical, IR, and radio data to study its star formation and obscured BH accretion. We name it *el Ascua*[24] given its red color, strong mid-IR emission from hot dust, and powerful accretion luminosity. In a forthcoming paper (A. P. Cloonan et al. in prep.), we will leverage the unprecedentedly wide area from MINERVA of deep MIRI imaging in ≥ 4 bands to study a large sample of X-ray-weak and/or CT AGN from $0 < z < 4$. When deriving physical properties, we assume the *Planck* cosmology from Planck Collaboration et al. (2020) with $H_0 = 67.66\,{\rm km\,s^{-1}\,Mpc^{-1}}$ and $\Omega_{m,0} = 0.30966$.

2. DATA AND ANALYSIS

2.1. *MINERVA NIRCam and MIRI*

MINERVA covers several legacy fields with deep imaging in both NIRCam medium bands and in multiple mid-IR filters with MIRI. For the purposes of measuring distant dusty galaxies, this dataset combines fine spectral sampling of the dust-attenuated stellar bump in the rest-optical with multi-band sampling of the rest-frame MIR. We can therefore disentangle PAHs from the dusty torus of the AGN in the mid-IR with significantly greater accuracy and precision on the photometric redshift.

Imaging of the UDS field with the broad-band filters from NIRCam, as well as two MIRI filters (F770W, F1800W) out of four, comes from the Public Release IMaging for Extragalactic Research (PRIMER) treasury program (GO-1837, PI: Dunlop; C. T. Donnan et al. 2024). MINERVA builds upon PRIMER in UDS by adding eight NIRCam medium bands and two additional MIRI filters (F1280W, F1500W), with a total area of 125 arcmin^2 imaged with all four MIRI filters. The archival *HST* data and new NIRCam data are reduced using `grizli` and following a similar strategy as in G. T. E. Sarrouh et al. (2026). More details of the NIRCam reductions can be found in S. E. Cutler et al. (2026) and in a subsequent paper (L. Robbins, et al. in prep.). The MIRI data from both PRIMER and MINERVA are reduced with a strategy based on the "super background" subtraction method introduced by S. Alberts et al. (2024). The full details of our data reduction strategy will be detailed in a subsequent paper (N. Martis et al. in prep.).

Photometric catalogs are first produced with NIRCam using a modified version of `aperpy`, and a brief overview of the method can be found in Section 2.2 of S. E. Cutler et al. (2026). Photometric redshifts are fit to the NIRCam photometry with EAzY (G. B. Brammer et al. 2008) with multiple sets of templates; in this paper, we use the redshift catalog created with the `sfhz_blue_agn` templates. A morphology catalog is constructed from the NIRCam catalog following the method from Y. Zhang et al. (2026), who fit single Sérsic profiles using the `pysersic` code. Finally, photometry in each MIRI filter is measured for each NIRCam source via a fixed-aperture measurement of the color between the MIRI image and the F444W image (PSF-matched to the MIRI resolution; e.g., R. Quadri et al. 2007). The strategy for full NIRCam+MIRI photometric catalogs will be detailed by Y. Asada et al. (in prep.).

2.2. *Ancillary Data*

In our analysis, we leverage archival coverage of the UDS field from *Chandra*, *Spitzer*, the Atacama Large Millimeter Array (ALMA), and the Karl Jansky Very Large Array (VLA). The *HST* and *Spitzer* data provide additional constraints on the UV-optical stellar bump and the mid-IR continuum from AGN and PAHs, while the ALMA coverage in Band 7 (from program 2015.1.01074.S; PI: Inami) places a constraint on the cold dust content and the total IR luminosity. With the X-ray data from the XUDS survey (D. D. Kocevski et al. 2018), we can verify CT obscuration, and the 1.4 GHz radio data from VLA (C. Simpson et al. 2006; B.

[24] "The Ember" in Spanish.

Zhang et al. 2025) probes the synchrotron emission which can be from star formation or from AGN-driven jets.

We obtain archival *Spitzer* and VLA fluxes from the NASA/IPAC Extragalactic Database. For the ALMA flux at 870 μm, we use the `PyBSDF` code to fit a single 2D Gaussian (with axis ratios of $a/b < 1$ allowed) to the light profile. This surface brightness fit gives a measurement of the total flux observed in an interferometric map, which we include in order to model the panchromatic spectral energy distributions (SEDs).

2.3. *SED Fitting with `CIGALE`*

We use `CIGALE` (M. Boquien et al. 2019; G. Yang et al. 2020) to model the UV-to-IR SEDs of galaxies in the MINERVA UDS catalog, including the rest-MIR dust emission both from PAHs and the warm dusty torus of an AGN. A full description of the SED modeling and AGN selection in MINERVA with `CIGALE` will be presented by E. Vidal et al. (in prep.), and we briefly outline the approach here. The redshifts are fixed to the best-fit photometric redshifts from the EAzY catalog using the `sfhz_blue_agn` templates. We adopt the set of priors used by G. Yang et al. (2023); C.-T. Ling et al. (2024, 2026); C.-A. Hsieh et al. (2025); T.-E. Bulichi et al. (2026); K. Hamblin et al. (2026); D. Lyon et al. (2026) to jointly fit galaxy+AGN emission observed with MIRI. The core ingredients are as follows: a delayed-tau star formation history model, the initial mass function from G. Chabrier (2003), the nebular emission model from J. A. Villa-Vélez et al. (2021), the dust attenuation model from D. Calzetti et al. (2000), the ISM dust emission model from B. T. Draine et al. (2014), and the `SKIRTOR` model for AGN emission from a clumpy torus (M. Stalevski et al. 2012, 2016). These `CIGALE` fits provide mid-IR AGN fractions, AGN luminosities, galaxy stellar masses, and star formation rates. For this paper (see Section 3), we add the photometry from *Spitzer*, ALMA, and the VLA, and then we repeat `CIGALE` fitting for *el Ascua* to improve the measurement of the IR luminosity and AGN accretion power.

3. SEARCHING FOR CT AGN

We select CT AGN in the MINERVA UDS catalog by comparing the intrinsic 6 μm AGN luminosity to the observed 2 – 10 keV X-ray luminosity. The mid-IR luminosity is given directly by the AGN model component in `CIGALE`, corrected for dust attenuation which is significant in the dustiest systems (M. Stalevski et al. 2016; G. Yang et al. 2020). The observed X-ray luminosity is uncorrected for gas absorption and is sensitive to N_H. The ratio between the two is therefore an excellent tracer for heavy obscuration, especially where direct X-ray detections are not available as is often true for CT AGN at $z > 0$ (e.g., G. B. Lansbury et al. 2015; R. C. Hickox & D. M. Alexander 2018; J. Lyu et al. 2024; R. Uematsu et al. 2025). Below, we describe our method for computing upper limits on the 2 – 10 keV X-ray luminosity, and we then outline our selection method for CT AGN.

3.1. *Upper limits on X-ray luminosity*

We focus on MIRI sources which are undetected in the X-ray maps. Therefore, upper limits on the uncorrected (i.e., absorbed) X-ray luminosity from rest-frame 2 – 10 keV are required, and we use the `aplimits`[25] routine from the `CIAO` and `CALDB` packages for *Chandra* data analysis. In the broad 0.5 – 7 keV band, we estimate the rate of background photon counts averaged over exposure time, telescope area, and solid angle (i.e., in units of counts cm^{-2} s^{-1} arcsec^{-2}) by summing the counts over a large source-free region in the X-ray map and dividing that number by the median exposure map value (which has units of cm^2 s) and by the solid angle of the region. The `aplimits` code uses this background rate to measure the minimum number of counts needed in the source aperture for detection, given a source aperture size and desired rates of false positives (where background noise exceeds the detection limit) and false negatives (where a source with exactly the flux upper limit is not flagged). We require a false positive rate of 0.23%, which corresponds to a 3σ Gaussian upper limit (V. L. Kashyap et al. 2010), and a false negative rate of 50%. We compute with an aperture of radius 3.″ and a monochromatic energy of 2.3 keV over the broad band, giving us an estimate on the upper limit on the observed-frame 0.5 – 7 keV flux.

We extrapolate these upper limits on flux to the rest-frame 2 – 10 keV range following the method from C. Ricci et al. (2021). We assume an X-ray spectrum $N(E) \propto E^{-\Gamma}$, where $\Gamma = 1.8$ is the photon index. This value for Γ is typical for broad-line and unobscured AGN (e.g., A. Del Moro et al. 2017), meaning that this model roughly corresponds to the maximally allowed spectrum for an unobscured and undetected source. We scale this mock spectrum to match each source's integrated upper limit over the observed 0.5 – 7 keV, and we then integrate over the rest-frame 2 – 10 keV range, and we then convert to a luminosity using the expected photon energy value (≈ 4.2 keV) from the mock spectrum over that energy range.

3.2. *An Extreme CT AGN*

From the initial catalog of 4632 MIRI-detected sources (i.e., $S/N > 5$ in at least 2 MIRI bands) in MINERVA UDS, the criteria which we use to select CT AGN are as follows:

- $\chi^2_\nu < 3$ for the best-fit SEDs from `CIGALE`, giving 4539 sources.

[25] https://cxc.cfa.harvard.edu/ciao/ahelp/aplimits.html

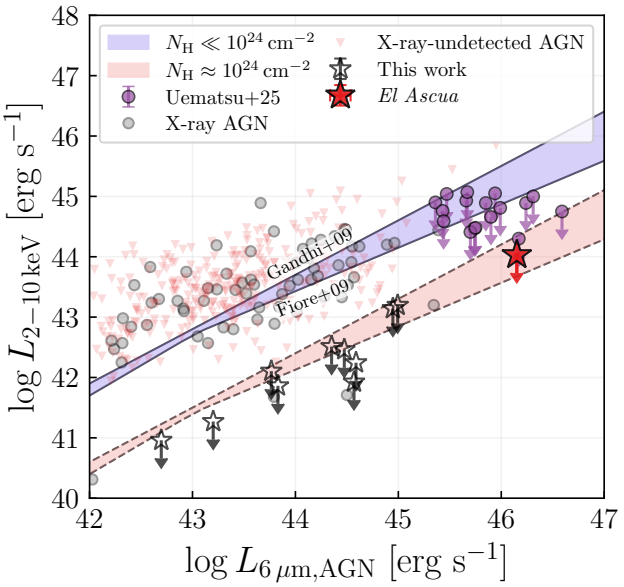


Figure 1. The discovery of a remarkably mid-IR bright ($L_{6\,\mu\mathrm{m,AGN}} \gtrsim 10^{46}$ erg s^{-1}) CT AGN candidate (*el Ascua*; red star) from a larger sample of CT AGN (shown with black stars). This plot shows the observed X-ray luminosity as a function of the intrinsic 6 μm AGN luminosity as obtained from SED fitting. The log-linear relation for unobscured (or Compton-thin) AGN is shown in light blue, as a shaded region between two different estimates from P. Gandhi et al. (2009) and F. Fiore et al. (2009). X-ray detected AGN in UDS which were detected with MINERVA MIRI imaging are shown as gray dots which roughly follows the shaded region for unobscured AGN. The relation for AGN with absorption of $N_H \approx 10^{24}$ cm^{-2} is shown in light red, and it corresponds to a normalization factor of ≈ 20 fainter in the X-ray luminosity (G. B. Lansbury et al. 2015). A sample of obscured candidate AGN in the COSMOS field are shown as purple dots (R. Uematsu et al. 2025).

- $f_{\mathrm{AGN}} \geq 0.3$ from CIGALE, i.e., the AGN contributes at least 30% of the emission between $3-30$ μm. This selection gives 451 AGN identified via the contribution of the dusty torus to the mid-IR.
- The nearest neighbor in the X-ray catalog (D. D. Kocevski et al. 2018) is located more than $3''$ away, giving 375 AGN which are simultaneously bright in the mid-IR and undetected in the X-ray.
- The source lies below the P. Gandhi et al. (2009) log-linear relation in $L_{6\,\mu\mathrm{m}} - L_{2-10\,\mathrm{keV}}$ normalized for CT absorption, giving 11 sources from the MIRI AGN catalog which we identify as CT AGN. The relation from F. Fiore et al. (2009) is slightly more restrictive, and other studies have found that sources between these two relations tend to have CT absorbing material of $N_H \approx 10^{24}$ cm^{-2} or slightly denser (e.g., G. B. Lansbury et al. 2015). The upper limits on $L_{2-10\,\mathrm{keV}}$ are computed as described above.

To summarize, we identify CT AGN as MIRI-bright, X-ray-undetected AGN where the upper limit on $L_{6\,\mu\mathrm{m}} - L_{2-10\,\mathrm{keV}}$ is sufficiently low to place the source below a predicted and empirically verified CT threshold.

From the final CT sample, we find one CT AGN with a mid-IR luminosity of $\log\left(L_{6\,\mu\mathrm{m}}/\mathrm{erg\,s^{-1}}\right) \gtrsim 46$, much brighter than the others which have $\log\left(L_{6\,\mu\mathrm{m}}/\mathrm{erg\,s^{-1}}\right) \lesssim 45$. This source is *el Ascua* at $z_{\mathrm{phot}} = 3.78^{+0.01}_{-0.03}$, and we present it and the rest of the CT sample in the $L_{6\,\mu\mathrm{m}} - L_{2-10\,\mathrm{keV}}$ parameter space in Figure 1. Notably, *el Ascua* has a similar AGN luminosity to a set of AGN-hosting SMGs studied by R. Uematsu et al. (2025) in the COSMOS field. However, the X-ray constraints are stronger for *el Ascua* than for the COSMOS sample, allowing us to more confidently identify CT obscuration.

We investigate how the posterior on photometric redshift impacts the upper limit on the X-ray luminosity. If the uncertainty is sufficiently large towards higher redshift, it can bias the limit upward and weaken the constraint on the X-ray obscuration provided by the $L_{6\,\mu\mathrm{m}} - L_{2-10\,\mathrm{keV}}$ parameter space. For *el Ascua*, the 95% confidence interval in redshift is $z_{\mathrm{phot}} = 3.78^{+0.02}_{-0.18}$. If we set the redshift to the 97.5% value of ≈ 3.80, we find that the upper limit on $L_{2-10\,\mathrm{keV}}$ increases by 0.004 dex, remaining below the expected CT threshold shown in Figure 1. We therefore conclude that the redshift uncertainty does not affect the interpretation that *el Ascua* is CT.

For reference, we also plot X-ray AGN in the UDS MINERVA MIRI footprint. We match X-ray sources to the catalog of MIRI sources with best-fit SEDs of $\chi^2_\nu < 3$ by requiring that the X-ray and *JWST* positions are within $1''$ of each other. Qualitatively, we find that the X-ray AGN are consistent with the known Compton-thin scaling relations from F. Fiore et al. (2009) and P. Gandhi et al. (2009), confirming that our method identifies X-ray-weak sources including CT AGN. Of the X-ray-detected AGN, two are CT given their mid-IR luminosity, leading to a sample size of 13 CT AGN in MINERVA/UDS. In a future paper (A. P. Cloonan et al. in prep.), we will study the full sample of CT AGN and their host galaxy properties in MINERVA.

4. SOURCE PROPERTIES AND DISCUSSION

We present the best-fit CIGALE SED from the rest-UV to the far-IR alongside image cutouts from X-ray to radio in Figure 2. The SED fit to the rest-frame mid-IR (probed by MIRI and *Spitzer* 24 μm) provides strong evidence of hot dust emission as found in obscured AGN (R. C. Hickox & D. M. Alexander 2018), with an estimated AGN fraction of $\approx 90\%$ over $3-30$ μm. The inferred AGN fraction is similarly large over the full IR. As is typical for buried AGN in dusty galaxies we see faint, attenuated starlight in the rest-UV and optical, and the absorbed starlight is reprocessed as

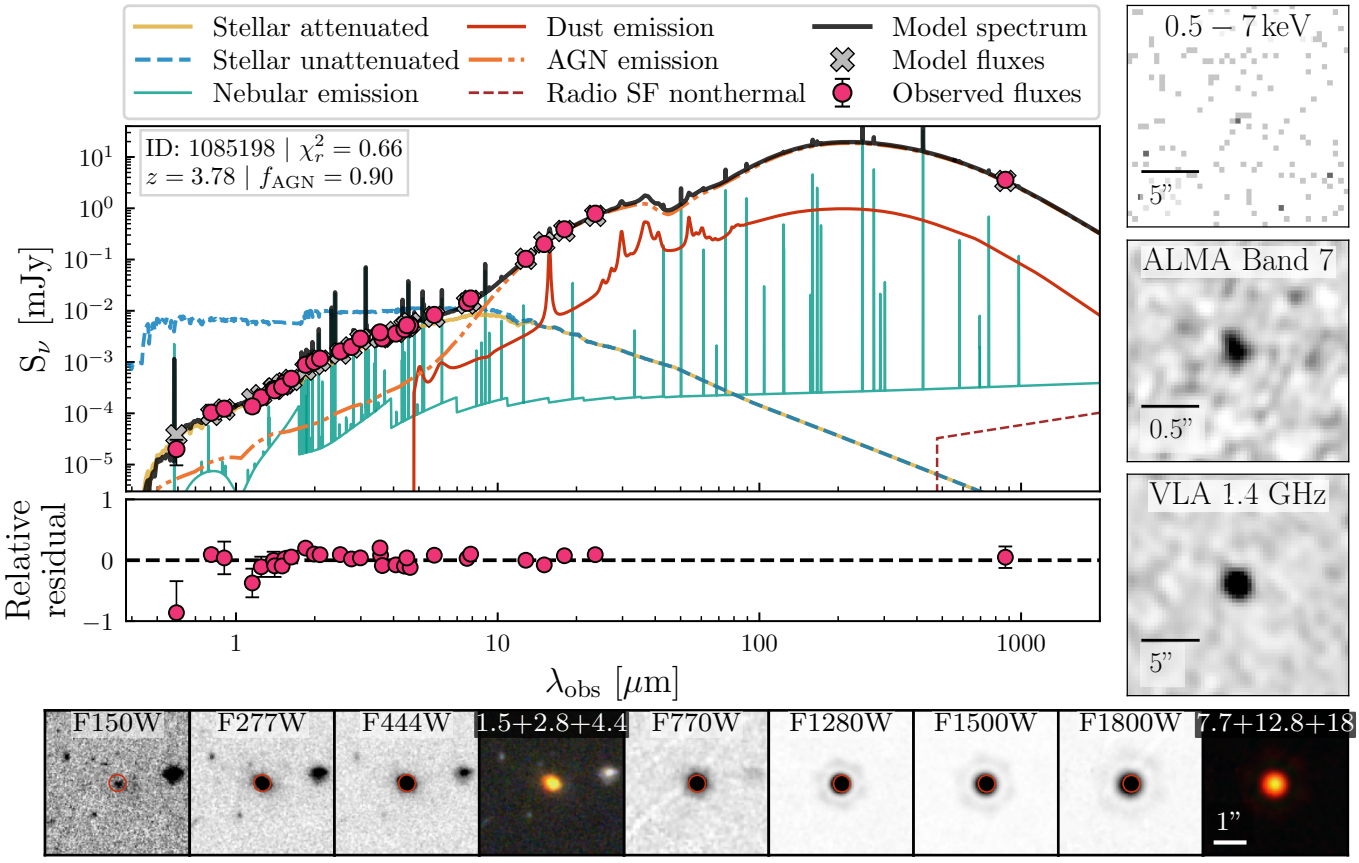


Figure 2. The best-fit SED from CIGALE and image cutouts in *JWST* filters, *Chandra* 0.5 – 2 keV, ALMA Band 7, and VLA 1.4 GHz. We also present a NIRCam RGB image using F150W (1.5 μm), F277W (2.8 μm), and F444W (4.4 μm); and a MIRI RGB using F770W (7.7 μm), F1280W (12.8 μm), and F1800W (18 μm). Both the SED and the *JWST* cutouts show a luminous mid-IR AGN and dust-attenuated starlight in the rest-UV and optical. The ALMA Band 7 map shows compact cold dust emission, and the AGN is undetected by *Chandra*. The mid-IR brightness combined with the inferred X-ray flux upper limit suggest CT obscuration. We also find a radio excess at 1.4 GHz with our updated measurement of the total IR luminosity. This excess is likely AGN-driven, meaning that *el Ascua* may be a rare radio-loud CT AGN.

IR dust emission. Observations of the far-IR spectral peak are necessary to study the extent to which the observed cold dust emission is driven by the AGN as opposed to star formation. The observed X-ray flux is below the detection limit from the background, while the source is strongly detected at 1.4 GHz. The half-light radius in F200W from the morphology catalog is $1.86^{+0.12}_{-0.12}$ kpc, which is near the median for massive star-forming galaxies at $3 < z < 4$ (L. Chen et al. 2026). In F444W the half-light radius is $1.20^{+0.01}_{-0.02}$ kpc, indicating that *el Ascua* is not a little red dot as its rest-optical flux is more extended than the typical < 0.1 kpc for LRDs (J. F. W. Baggen et al. 2026; A. P. Cloonan et al. 2026).

The properties of *el Ascua* and its host galaxy are measured directly from the CIGALE SED fitting; the MIR AGN fraction ($f_{\rm AGN}$), the accretion power of the AGN ($L_{\rm acc}$), the stellar mass ($M_\star$) and star formation rate (SFR; over the last 100Myr) of the host galaxy, and the total IR luminosity of the source (galaxy+AGN) over $8 - 1000\,\mu$m. The values of these properties are listed in Table 1, along with basic information including sky coordinates and photometric redshift. The accretion power ($L_{\rm acc}$) provided by CIGALE is defined as the intrinsic (i.e., corrected for absorption) luminosity of the accretion disk averaged over viewing angle.

El Ascua is among the most extreme AGN at $z \sim 4$ which belong to the missing obscured population known from the cosmic X-ray background (e.g., Y. Ueda et al. 2003) and from comparing MIR and X-ray luminosity functions (LFs; e.g., J. Runburg et al. 2022; T.-E. Bulichi et al. 2026). Unsurprisingly, with $\log\left(L_{\rm acc}/{\rm erg\ s^{-1}}\right) \sim 47$, it falls at the luminous end of the MIRI AGN LF at $z \sim 4$. However, the MIR and X-ray LFs at $z \sim 4$ begin to converge around $\log\left(L_{\rm acc}/{\rm erg\ s^{-1}}\right) \sim 47$; in other words, the fraction of missing X-ray-faint AGN decreases as $L_{\rm acc}$ increases toward $\log\left(L_{\rm acc}/{\rm erg\ s^{-1}}\right) \sim 47$ (T.-E. Bulichi et al. 2026). We argue that while CT AGN are likely common overall at $z \sim 4$, CT AGN of such high luminosity as *el Ascua* are statistically rare.

Additionally, *el Ascua* is of similar luminosity to other remarkably bright CT AGN at $z \sim 4$ (e.g., R. Gilli et al. 2014; F. Vito et al. 2020; I. Villani et al. 2026), and it is slightly

Table 1. A number of observables and physical properties of *el Ascua*, the extreme CT AGN reported in this work. The rows are in order as follows: the right ascension, the declination, the photometric redshift ($z_{\rm phot}$), the AGN fraction over $3-30\,\mu$m ($f_{\rm AGN}$), the sub-mm flux at 870 μm from ALMA, the mid-IR continuum luminosity at 6 μm from the AGN component ($L_{6\,\mu{\rm m,AGN}}$) and the total SED ($L_{6\,\mu{\rm m,tot}}$), the X-ray luminosity over $2-10\,$keV ($L_{2-10\,{\rm keV}}$), the accretion power (or the angle-averaged intrinsic disk luminosity; $L_{\rm acc}$), the black hole accretion rate (BHAR) assuming a radiative efficiency of $\epsilon = 0.1$, the host galaxy stellar mass ($M_\star$), the star formation rate (SFR) over the last 100 Myr from the SED fitting, the integrated IR luminosity over $8-1000\,\mu$m ($L_{\rm IR}$), the component of $L_{\rm IR}$ from star formation ($L_{\rm IR,SF}$), the radio power at 1.4 GHz ($P_{1.4\,{\rm GHz}}$), and a log-ratio ($q_{\rm TIR}$) between $L_{\rm IR,SF}$ and $P_{1.4\,{\rm GHz}}$.

Property		Value
RA	(J2000)	34.35823432
Dec	(J2000)	-5.24091976
$z_{\rm phot}$		$3.78^{+0.01}_{-0.03}$
$f_{\rm AGN}$	$(3-30\,\mu{\rm m})$	0.90 ± 0.01
$F_{870\,\mu{\rm m}}$	(mJy)	3.59 ± 0.64
$\log L_{6\,\mu{\rm m,AGN}}$	(erg s^{-1})	46.15 ± 0.02
$\log L_{6\,\mu{\rm m,tot}}$	(erg s^{-1})	46.19 ± 0.02
$\log L_{2-10\,{\rm keV}}$	(erg s^{-1})	<44.03
$\log L_{\rm acc}$	(erg s^{-1})	47.12 ± 0.58
BHAR($\epsilon=0.1$)	($M_\odot$yr^{-1})	20.4 ± 3.1
$\log M_\star$	($M_\odot$)	10.82 ± 0.57
SFR$_{\rm SED}$	($M_\odot$yr^{-1})	157 ± 8
$\log L_{\rm IR}$	($L_\odot$; $8-1000\,\mu$m)	13.25 ± 0.16
$\log L_{\rm IR,SF}$	($L_\odot$; $8-1000\,\mu$m)	12.11 ± 0.16
$\log P_{1.4\,{\rm GHz}}$	(W Hz^{-1})	25.46 ± 0.03
$q_{\rm TIR}$		0.68 ± 0.16

less luminous than hot dust-obscured galaxies (hot DOGs; L. Fan et al. 2016; J. Wu et al. 2018; G. Li et al. 2024) and the rare 'extremely red quasars' (Y. Ma et al. 2024). Compared to local CT AGN, *el Ascua* is one or two orders of magnitude more luminous (e.g., L. Spinoglio et al. 2022, 2024; A. Annuar et al. 2025).

From $L_{\rm acc}$, we compute the black hole accretion rate (BHAR) following the formalism used by A. Marconi et al. (2004) and G. Yang et al. (2023):

$$\mathrm{BHAR} = \frac{L_{\rm acc}(1-\epsilon)}{\epsilon c^2} \tag{1}$$

where ϵ is the radiative efficiency and c is the speed of light. This formalism for BHAR is derived by subtracting the fraction of mass converted into radiation from the total accreted mass, assuming spherical accretion. For *el Ascua*, we estimate BHAR $= 20.4\pm3.1\,{\rm M_\odot yr^{-1}}$ assuming a population-average $\epsilon\approx0.1$. If we instead assume a theoretical maximum of $\epsilon\approx0.42$ (K. S. Thorne 1974; T. T. Ananna et al. 2020) for a rapidly rotating Kerr black hole, we find BHAR $= 3.23\pm0.24\,{\rm M_\odot yr^{-1}}$.

The SMBH in *el Ascua* is growing more quickly than anticipated from the galaxy stellar mass and SFR. Even with the upper limit of $\epsilon\approx0.42$ from theory, we find a large ratio of BHAR/SFR $= 0.020\pm0.002$. For reference, M. Stone et al. (2022) find a characteristic BHAR/SFR of ~0.01 for a stack of LIRGs at $z\sim0$ with $f_{\rm AGN}\approx0.96$. A related metric, the specific BHAR (sBHAR), paints the same picture and can be defined as a modified ratio of AGN accretion power to galaxy stellar mass (M. Habouzit et al. 2019):

$$\mathrm{sBHAR} = \frac{L_{\rm acc}}{10^{38}\,{\rm erg\ s^{-1}}} \times \left(\frac{0.002M_\star}{M_\odot}\right)^{-1}. \tag{2}$$

We find sBHAR $= 9.95\pm1.1$ for *el Ascua*. This value falls on the tail of the sBHAR distribution function for star-forming galaxies of $10<\log M_\star<11$ at $3<z<4$, which has an average in the range of $\langle\mathrm{sBHAR}\rangle\sim0.1-0.3$ and begins to decrease dramatically at sBHAR $\gtrsim0.5$ (J. Aird et al. 2018; M. Habouzit et al. 2019). Large BHAR/SFR and sBHAR values are often associated with accretion rates nearing or exceeding the Eddington limit (J. Aird et al. 2018).

We make a rough estimate for the Eddington ratio $\lambda_{\rm Edd}\equiv L_{\rm acc}/L_{\rm Edd}\propto M_{\rm BH}^{-1}$ (A. Marconi et al. 2004) by assuming that *el Ascua* falls within 3σ of the $M_{\rm BH}-M_\star$ scaling relation at $3<z<4$ (J. Kormendy & L. C. Ho 2013; J. E. Greene et al. 2020). If we suppose an average mass ratio of $\langle M_{\rm BH}/M_\star\rangle\sim10^{-3}$ with an intrinsic scatter of $\sigma_{\rm int}\approx0.9$dex, as measured by B. L. Jones et al. (2025), we find an extremely conservative 3σ upper limit of $\log\left(M_{\rm BH}/M_\odot\right)<10.52$ given a stellar mass of $\log\left(M_\star/M_\odot\right)\approx10.82$. Paired with the AGN accretion power, this upper limit corresponds to a conservative lower limit on the Eddington ratio of $\lambda_{\rm Edd}>0.031$. We note that we cannot claim that the black hole is as remarkably massive as $\log\left(M_{\rm BH}/M_\odot\right)\sim10.5$, as more precise estimates of $M_{\rm BH}$ are not available with current data. Indeed, the mass is most likely significantly lower given the SMBH mass function. The MIRI imaging in UDS from PRIMER and MINERVA probes a comoving volume of $\approx3.4\times10^6\,{\rm Mpc^3}$ over $3.5<z<4.25$, whereas the mass function predicts ~1 BH with $\log\left(M_{\rm BH}/M_\odot\right)\sim10.5$ over a much larger comoving volume of $\sim10^9\,{\rm Mpc^3}$ in the same redshift bin (e.g., W. He et al. 2024). We therefore anticipate that the Eddington ratio of *el Ascua* is significantly higher than the lower limit we find. Follow-up spectroscopy with NIRSpec can measure $M_{\rm BH}$ and test that expectation.

From these various diagnostics of BH accretion, we conclude that *el Ascua* might be nearing the peak of a phase of obscured BH growth before AGN feedback expels the ob-

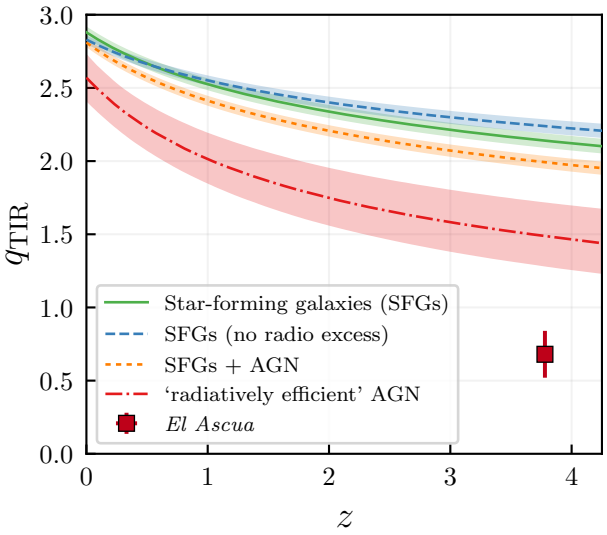


Figure 3. The observed ratio for *el Ascua* between SF-driven IR luminosity and the 1.4 GHz radio power, measured with CIGALE, is consistent with an AGN-driven radio excess. We present empirical curves from J. Delhaize et al. (2017) for the ratio $q_{\rm TIR}(z)$ as a function of redshift in different source populations. Star-forming galaxies are shown in blue and green, while all sources are shown in orange and 'radiatively efficient' AGN are shown in red. We note that this population of radiatively efficient AGN are mostly radio-quiet (I. Delvecchio et al. 2017; V. Smolčić et al. 2017).

scuring material. Pairing the conservative lower limits on $\lambda_{\rm Edd}$ with the inferred $N_H > 10^{24}\,{\rm cm}^{-2}$, we find that *el Ascua* lies near the end of 'Stage 2' in the radiation-regulated unification model outlined by C. Ricci et al. (2017, 2023). In this framework, SMBHs begin in a quiescent, low-$\lambda_{\rm Edd}$ state (Stage 1), and then accretion begins with an obscured phase where both $\lambda_{\rm Edd}$ and N_H increase as the SMBH grows. Then, after surpassing the 'effective' Eddington limit $\lambda_{\rm eff}(N_H)$ for the dusty gas (which is a function of column density), AGN radiative feedback becomes much more efficient. The AGN at this point enters a brief 'blowout' phase (Stage 3) before transitioning into an unobscured quasar with high $\lambda_{\rm Edd}$ and low N_H (Stage 4). Most hot DOGs and other hyper-luminous reddened quasars are in or nearing the blowout phase (e.g., J. Wu et al. 2018; H. D. Jun et al. 2021; A. Kayal & V. Singh 2024; F. Zou et al. 2025). With *el Ascua* located in the extreme end of Stage 2 but slightly less luminous than most hot DOGs, the AGN could be nearing the effective Eddington limit and therefore located in a pre-hot DOG phase.

4.1. *The radio emission and possible radio-loudness*

Star-forming galaxies exhibit a strong correlation between IR and radio luminosities, and the ratio between them can provide an additional signature of AGN activity in the form of a radio excess (e.g., A. Del Moro et al. 2013; J. Delhaize et al. 2017; B. Zhang et al. 2025). A. Sajina et al. (2007) find that a large fraction ($\sim 40\%$) of dusty mid-IR AGN with silicate absorption at 9.7 μm are radio loud. We find that *el Ascua* is strongly detected at 1.4 GHz with the VLA (C. Simpson et al. 2006). To investigate whether *el Ascua* is radio-loud or quiet, we measure the ratio $q_{\rm TIR}$ between the total IR and radio luminosities as:

$$q_{\rm TIR} = \log\left(\frac{L_{\rm IR,SF}}{3.75\times10^{12}\,{\rm Hz}}\right) - \log\left(\frac{P_{1.4\,{\rm GHz}}}{{\rm W\,Hz^{-1}}}\right), \quad (3)$$

where $L_{\rm IR,SF}$ is the IR luminosity in W due to star formation (from the SED fit), and $P_{1.4\,{\rm GHz}}$ is the radio power at 1.4 GHz in $\rm W\,Hz^{-1}$. We then compare to the redshift evolution $q_{\rm TIR}(z)$ for different source populations as measured by J. Delhaize et al. (2017), namely star-forming galaxies and 'radiatively efficient' AGN. This population of AGN is a union of mid-IR-, X-ray-, and SED-selected AGN and they are mostly radio-quiet (I. Delvecchio et al. 2017; V. Smolčić et al. 2017). The results are shown in Figure 3.

We find that *el Ascua* has a radio excess; i.e., its $q_{\rm TIR}$ value is significantly lower than predicted for luminous AGN at its redshift. The synchrotron radiation is likely driven by the AGN, as star formation does not account for the observed power at 1.4 GHz. We conclude that *el Ascua* is likely a radio-loud AGN, which matches the result from B. Zhang et al. (2025) who include *el Ascua* in their catalog of radio AGN identified via a similar technique with the IR–radio correlation. Radio-loud CT AGN are notably rare with only a handful of confirmed sources (S. M. LaMassa et al. 2023). If *el Ascua* is indeed radio-loud, then it may be the most distant example yet known, and it would provide a novel opportunity to study the obscuring material in AGN in the distant universe.

5. SUMMARY

In this work we present the discovery of a remarkably luminous CT AGN at $z \approx 3.78$ with multi-band MIRI imaging from the MINERVA survey (A. Muzzin et al. 2025) and archival X-ray data from the XUDS survey (D. D. Kocevski et al. 2018). Our results and interpretations are summarized as follows:

- We find that *el Ascua* is among the most luminous mid-IR AGN in UDS, with $\log\left(L_{6\,\mu{\rm m}}/{\rm erg\,s^{-1}}\right) \approx 46.15 \pm 0.02$. Our X-ray measurement of $\log\left(L_{2-10\,{\rm keV}}/{\rm erg\,s^{-1}}\right) < 44.03$ places *el Ascua* on the $L_{6\,\mu{\rm m}} - L_{2-10\,{\rm keV}}$ scaling relation expected for AGN with gaseous obscuring material of column density $N_H \approx 10^{24}\,{\rm cm}^{-2}$ (F. Fiore et al. 2009; P. Gandhi et al. 2009; G. B. Lansbury et al. 2015). This result suggests that the AGN is Compton-thick.

- From SED fitting with CIGALE, we find that *el Ascua* has a powerful accretion luminosity of

$\log\left(L_{\rm acc}/{\rm erg\ s^{-1}}\right) \approx 47.12 \pm 0.58$, at the extremely high end of the AGN luminosity function at $z \sim 4$ (T.-E. Bulichi et al. 2026). Given the host galaxy stellar masses and SFR, this luminosity corresponds to large BHAR/SFR and sBHAR values (and likely a high $\lambda_{\rm Edd}$ value as well) when compared to the AGN population at this redshift. These physical properties characterize *el Ascua* as nearing or at a peak phase of heavily obscured SMBH growth, where accretion accelerates and the column density increases until powerful AGN feedback clears the obscuring material (C. Ricci et al. 2017, 2023). This phase is comparable to the stage of SMBH growth observed in hot DOGs (e.g., J. Wu et al. 2018; F. Zou et al. 2025).

- We measure the ratio between the IR and radio luminosities and find *el Ascua* exhibits a radio-excess consistent with AGN-driven synchrotron radiation. An excess indicates that *el Ascua* may be among the most distant radio-loud CT AGN known in the universe (S. M. LaMassa et al. 2023).

Though located in the well-studied UDS field (A. Lawrence et al. 2007), *el Ascua* had not been flagged as a mid-IR-luminous AGN of any type previously. Its discovery with *JWST* demonstrates the power that MIRI provides to the community for directly confirming powerful, heavily obscured AGN which we have long understood as missing from the census of SMBH growth.

Remarkably luminous sources such as *el Ascua* are key laboratories for detailed study of heavily obscured AGN in the early universe. Follow-up NIRSpec and MIRI spectroscopy can corroborate the mid-IR evidence of AGN activity with emission line diagnostics of the narrow-line region (A. Calabrò et al. 2023), constrain the black hole mass with broad emission lines, and measure outflow kinematics to probe AGN feedback. In the further future, the far-IR PRIMA mission (J. Glenn et al. 2025) will measure the full IR SED with narrow-band photometry and provide rest-frame mid-IR spectroscopy at $z \sim 4$, directly measuring the accretion power (A. Sajina et al. 2022; L. Spinoglio et al. 2022) and disentangling dust temperature components for heavily obscured AGN in the early universe. These rich, unprecedented IR datasets will map the connection between obscured black hole accretion and feedback (C. Ricci et al. 2017, 2023) at high redshift.

ACKNOWLEDGMENTS

The authors note that no generative AI was used in the preparation of this manuscript, including the analysis described therein.

APC warmly thanks Pallavi Patil, Teodora-Elena Bulichi, Andrew Mizener, Leonardo Barba, and Catalina Zamora for helpful discussions, and they recognize the generous support of the National Science Foundation through the NSF Graduate Research Fellowship Program. APC also warmly acknowledges Aurelian Capello, who helped choose the name of the discovered object.

DM acknowledges generous support from the Leonard and Jane Holmes Bernstein Professorship in Evolutionary Science.

PD warmly acknowledges support from an NSERC discovery grant (RGPIN-2025-06182).

This work is based in part on observations made with the NASA/ESA/CSA James Webb Space Telescope obtained from the Space Telescope Science Institute, which is operated by the Association of Universities for Research in Astronomy, Inc., under NASA contract NAS 5-26555. Financial support for program JWST-GO-7814 is gratefully acknowledged and is provided by NASA through grants from the Space Telescope Science Institute, which is operated by the Association of Universities for Research in Astronomy, Incorporated, under NASA contract NAS 5-03127. The data described here may be obtained from the MAST archive at doi:10.17909/cg7r-tq15. Computational resources for this work were provided by the University of Massachusetts Amherst's partnership with the Unity Research Computing Platform, a multi-institutional cluster led by the University of Massachusetts and the University of Rhode Island. The authors acknowledge the Tufts University High Performance Computing Cluster[26], which was utilized for the research reported in this paper. This research used the Canadian Advanced Network For Astronomy Research (CANFAR) operated in partnership by the Canadian Astronomy Data Centre and The Digital Research Alliance of Canada with support from the National Research Council of Canada, the Canadian Space Agency, CANARIE, and the Canadian Foundation for Innovation. The Cosmic Dawn Center is funded by the Danish National Research Foundation under grant DNRF140.

This research has made use of the NASA/IPAC Extragalactic Database, which is funded by the National Aeronautics and Space Administration and operated by the California Institute of Technology.

Facilities: JWST/NIRCam, JWST/MIRI

Software: `astropy` (Astropy Collaboration et al. 2013, 2018, 2022), `NumPy` (C. R. Harris et al. 2020), `matplotlib` (J. D. Hunter 2007), `SciPy` (P. Virtanen et al.

[26] https://it.tufts.edu/high-performance-computing

2020), CIGALE (M. Boquien et al. 2019; G. Yang et al. 2020)

REFERENCES

Aird, J., Coil, A. L., & Georgakakis, A. 2018, MNRAS, 474, 1225, doi: 10.1093/mnras/stx2700

Alberts, S., Lyu, J., Shivaei, I., et al. 2024, ApJ, 976, 224, doi: 10.3847/1538-4357/ad7396

Alexander, D. M., Chary, R.-R., Pope, A., et al. 2008, ApJ, 687, 835, doi: 10.1086/591928

Ananna, T. T., Treister, E., Urry, C. M., et al. 2019, ApJ, 871, 240, doi: 10.3847/1538-4357/aafb77

Ananna, T. T., Urry, C. M., Treister, E., et al. 2020, ApJ, 903, 85, doi: 10.3847/1538-4357/abb815

Annuar, A., Alexander, D. M., Gandhi, P., et al. 2025, MNRAS, 540, 3827, doi: 10.1093/mnras/staf956

Astropy Collaboration, Robitaille, T. P., Tollerud, E. J., et al. 2013, A&A, 558, A33, doi: 10.1051/0004-6361/201322068

Astropy Collaboration, Price-Whelan, A. M., Sipőcz, B. M., et al. 2018, AJ, 156, 123, doi: 10.3847/1538-3881/aabc4f

Astropy Collaboration, Price-Whelan, A. M., Lim, P. L., et al. 2022, ApJ, 935, 167, doi: 10.3847/1538-4357/ac7c74

Backhaus, B. E., Kirkpatrick, A., Hamblin, K., et al. 2026, arXiv e-prints, arXiv:2606.17146, doi: 10.48550/arXiv.2606.17146

Baggen, J. F. W., van Dokkum, P., Labbé, I., & Brammer, G. 2026, ApJL, 1006, L14, doi: 10.3847/2041-8213/ae82fe

Bauer, F. E., Yan, L., Sajina, A., & Alexander, D. M. 2010, ApJ, 710, 212, doi: 10.1088/0004-637X/710/1/212

Bauer, F. E., Arévalo, P., Walton, D. J., et al. 2015, ApJ, 812, 116, doi: 10.1088/0004-637X/812/2/116

Boquien, M., Burgarella, D., Roehlly, Y., et al. 2019, A&A, 622, A103, doi: 10.1051/0004-6361/201834156

Brammer, G. B., van Dokkum, P. G., & Coppi, P. 2008, ApJ, 686, 1503, doi: 10.1086/591786

Brightman, M., & Ueda, Y. 2012, MNRAS, 423, 702, doi: 10.1111/j.1365-2966.2012.20908.x

Buchner, J., Georgakakis, A., Nandra, K., et al. 2015, ApJ, 802, 89, doi: 10.1088/0004-637X/802/2/89

Bulichi, T.-E., Leung, G. C. K., Eilers, A.-C., et al. 2026, arXiv e-prints, arXiv:2603.22393, doi: 10.48550/arXiv.2603.22393

Burlon, D., Ajello, M., Greiner, J., et al. 2011, ApJ, 728, 58, doi: 10.1088/0004-637X/728/1/58

Calabrò, A., Pentericci, L., Feltre, A., et al. 2023, A&A, 679, A80, doi: 10.1051/0004-6361/202347190

Calzetti, D., Armus, L., Bohlin, R. C., et al. 2000, ApJ, 533, 682, doi: 10.1086/308692

Carroll, C. M., Ananna, T. T., Hickox, R. C., et al. 2023, ApJ, 950, 127, doi: 10.3847/1538-4357/acc402

Chabrier, G. 2003, PASP, 115, 763, doi: 10.1086/376392

Chen, L., Wang, T., Sun, H., et al. 2026, ApJL, 1002, L40, doi: 10.3847/2041-8213/ae5a93

Cloonan, A. P., Whitaker, K. E., Manning, S. M., et al. 2026, arXiv e-prints, arXiv:2603.24700, doi: 10.48550/arXiv.2603.24700

Comastri, A. 2004, in Astrophysics and Space Science Library, Vol. 308, Supermassive Black Holes in the Distant Universe, ed. A. J. Barger, 245, doi: 10.1007/978-1-4020-2471-9_8

Cutler, S. E., Robbins, L., Marchesini, D., et al. 2026, arXiv e-prints, arXiv:2606.02698, doi: 10.48550/arXiv.2606.02698

Daddi, E., Alexander, D. M., Dickinson, M., et al. 2007, ApJ, 670, 173, doi: 10.1086/521820

Del Moro, A., Alexander, D. M., Mullaney, J. R., et al. 2013, A&A, 549, A59, doi: 10.1051/0004-6361/201219880

Del Moro, A., Alexander, D. M., Bauer, F. E., et al. 2016, MNRAS, 456, 2105, doi: 10.1093/mnras/stv2748

Del Moro, A., Alexander, D. M., Aird, J. A., et al. 2017, ApJ, 849, 57, doi: 10.3847/1538-4357/aa9115

Delhaize, J., Smolčić, V., Delvecchio, I., et al. 2017, A&A, 602, A4, doi: 10.1051/0004-6361/201629430

Delvecchio, I., Smolčić, V., Zamorani, G., et al. 2017, A&A, 602, A3, doi: 10.1051/0004-6361/201629367

Donnan, C. T., McLure, R. J., Dunlop, J. S., et al. 2024, MNRAS, 533, 3222, doi: 10.1093/mnras/stae2037

Draine, B. T., Aniano, G., Krause, O., et al. 2014, ApJ, 780, 172, doi: 10.1088/0004-637X/780/2/172

Draper, A. R., & Ballantyne, D. R. 2010, ApJL, 715, L99, doi: 10.1088/2041-8205/715/2/L99

Falstad, N., Aalto, S., König, S., et al. 2021, A&A, 649, A105, doi: 10.1051/0004-6361/202039291

Fan, L., Han, Y., Fang, G., et al. 2016, ApJL, 822, L32, doi: 10.3847/2041-8205/822/2/L32

Fiore, F., Puccetti, S., Brusa, M., et al. 2009, ApJ, 693, 447, doi: 10.1088/0004-637X/693/1/447

Gandhi, P., Horst, H., Smette, A., et al. 2009, A&A, 502, 457, doi: 10.1051/0004-6361/200811368

Gilli, R., Comastri, A., & Hasinger, G. 2007, A&A, 463, 79, doi: 10.1051/0004-6361:20066334

Gilli, R., Norman, C., Vignali, C., et al. 2014, A&A, 562, A67, doi: 10.1051/0004-6361/201322892

Glenn, J., Meixner, M., Bradford, C. M., et al. 2025, Journal of Astronomical Telescopes, Instruments, and Systems, 11, 031628, doi: 10.1117/1.JATIS.11.3.031628

Goulding, A. D., Alexander, D. M., Bauer, F. E., et al. 2012, ApJ, 755, 5, doi: 10.1088/0004-637X/755/1/5

Greene, J. E., Strader, J., & Ho, L. C. 2020, ARA&A, 58, 257, doi: 10.1146/annurev-astro-032620-021835
Gruppioni, C., Pozzi, F., Rodighiero, G., et al. 2013, MNRAS, 432, 23, doi: 10.1093/mnras/stt308
Guo, X., Gu, Q., Fang, G., et al. 2025, A&A, 694, A241, doi: 10.1051/0004-6361/202452056
Habouzit, M., Genel, S., Somerville, R. S., et al. 2019, MNRAS, 484, 4413, doi: 10.1093/mnras/stz102
Hamblin, K., Kirkpatrick, A., Backhaus, B. E., et al. 2026, ApJ, 1002, 223, doi: 10.3847/1538-4357/ae4d3f
Harris, C. R., Millman, K. J., van der Walt, S. J., et al. 2020, Nature, 585, 357, doi: 10.1038/s41586-020-2649-2
He, W., Akiyama, M., Enoki, M., et al. 2024, ApJ, 962, 152, doi: 10.3847/1538-4357/ad1518
Hickox, R. C., & Alexander, D. M. 2018, ARA&A, 56, 625, doi: 10.1146/annurev-astro-081817-051803
Hsieh, C.-A., Goto, T., Ling, C.-T., et al. 2025, PASA, 42, e095, doi: 10.1017/pasa.2025.10055
Hunter, J. D. 2007, Computing in Science & Engineering, 9, 90, doi: 10.1109/MCSE.2007.55
Johnstone, M. A., Privon, G. C., Barcos-Muñoz, L., et al. 2025, ApJ, 985, 259, doi: 10.3847/1538-4357/adcecb
Jones, B. L., Kocevski, D. D., Pacucci, F., et al. 2025, arXiv e-prints, arXiv:2510.07376, doi: 10.48550/arXiv.2510.07376
Jun, H. D., Assef, R. J., Carroll, C. M., et al. 2021, ApJ, 906, 21, doi: 10.3847/1538-4357/abc629
Kashyap, V. L., van Dyk, D. A., Connors, A., et al. 2010, ApJ, 719, 900, doi: 10.1088/0004-637X/719/1/900
Kayal, A., & Singh, V. 2024, MNRAS, 531, 830, doi: 10.1093/mnras/stae1191
Kirkpatrick, A., Pope, A., Sajina, A., et al. 2015, ApJ, 814, 9, doi: 10.1088/0004-637X/814/1/9
Kirkpatrick, A., Pope, A., Alexander, D. M., et al. 2012, ApJ, 759, 139, doi: 10.1088/0004-637X/759/2/139
Kirkpatrick, A., Yang, G., Le Bail, A., et al. 2023, ApJL, 959, L7, doi: 10.3847/2041-8213/ad0b14
Kocevski, D. D., Hasinger, G., Brightman, M., et al. 2018, ApJS, 236, 48, doi: 10.3847/1538-4365/aab9b4
Kormendy, J., & Ho, L. C. 2013, ARA&A, 51, 511, doi: 10.1146/annurev-astro-082708-101811
Lacy, M., Petric, A. O., Sajina, A., et al. 2007, AJ, 133, 186, doi: 10.1086/509617
Lacy, M., & Sajina, A. 2020, Nature Astronomy, 4, 352, doi: 10.1038/s41550-020-1071-x
LaMassa, S. M., Yaqoob, T., Tzanavaris, P., et al. 2023, ApJ, 944, 152, doi: 10.3847/1538-4357/acb3bb
Lansbury, G. B., Gandhi, P., Alexander, D. M., et al. 2015, ApJ, 809, 115, doi: 10.1088/0004-637X/809/2/115
Lanzuisi, G., Civano, F., Marchesi, S., et al. 2018, MNRAS, 480, 2578, doi: 10.1093/mnras/sty2025
Lawrence, A., Warren, S. J., Almaini, O., et al. 2007, MNRAS, 379, 1599, doi: 10.1111/j.1365-2966.2007.12040.x
Li, G., Assef, R. J., Tsai, C.-W., et al. 2024, ApJ, 971, 40, doi: 10.3847/1538-4357/ad5317
Ling, C.-T., Goto, T., Kim, S. J., et al. 2026, PASP, 138, 014102, doi: 10.1088/1538-3873/ae2a6d
Ling, C.-T., Goto, T., Kim, S. J., et al. 2024, MNRAS, 528, 6025, doi: 10.1093/mnras/stae427
Lyon, D., Cowley, M., Pye, O., & Hopkins, A. 2026, PASA, 43, e024, doi: 10.1017/pasa.2026.10152
Lyu, J., & Rieke, G. 2022, Universe, 8, 304, doi: 10.3390/universe8060304
Lyu, J., Alberts, S., Rieke, G. H., et al. 2024, ApJ, 966, 229, doi: 10.3847/1538-4357/ad3643
Ma, Y., Goulding, A., Greene, J. E., et al. 2024, ApJ, 974, 225, doi: 10.3847/1538-4357/ad710c
Maiolino, R., Risaliti, G., Signorini, M., et al. 2025, MNRAS, 538, 1921, doi: 10.1093/mnras/staf359
Marconi, A., Risaliti, G., Gilli, R., et al. 2004, MNRAS, 351, 169, doi: 10.1111/j.1365-2966.2004.07765.x
Muzzin, A., Suess, K. A., Marchesini, D., et al. 2025, arXiv e-prints, arXiv:2507.19706, doi: 10.48550/arXiv.2507.19706
Nardini, E., & Risaliti, G. 2011, MNRAS, 415, 619, doi: 10.1111/j.1365-2966.2011.18732.x
Planck Collaboration, Aghanim, N., Akrami, Y., et al. 2020, A&A, 641, A6, doi: 10.1051/0004-6361/201833910
Pope, A., Chary, R.-R., Alexander, D. M., et al. 2008, ApJ, 675, 1171, doi: 10.1086/527030
Quadri, R., Marchesini, D., van Dokkum, P., et al. 2007, AJ, 134, 1103, doi: 10.1086/520330
Ricci, C., Trakhtenbrot, B., Koss, M. J., et al. 2017, Nature, 549, 488, doi: 10.1038/nature23906
Ricci, C., Privon, G. C., Pfeifle, R. W., et al. 2021, MNRAS, 506, 5935, doi: 10.1093/mnras/stab2052
Ricci, C., Ichikawa, K., Stalevski, M., et al. 2023, ApJ, 959, 27, doi: 10.3847/1538-4357/ad0733
Runburg, J., Farrah, D., Sajina, A., et al. 2022, ApJ, 924, 133, doi: 10.3847/1538-4357/ac37b8
Sajina, A., Lacy, M., & Pope, A. 2022, Universe, 8, 356, doi: 10.3390/universe8070356
Sajina, A., Yan, L., Lacy, M., & Huynh, M. 2007, ApJL, 667, L17, doi: 10.1086/522050
Sarrouh, G. T. E., Asada, Y., Martis, N. S., et al. 2026, ApJS, 282, 3, doi: 10.3847/1538-4365/ae1611
Simpson, C., Martínez-Sansigre, A., Rawlings, S., et al. 2006, MNRAS, 372, 741, doi: 10.1111/j.1365-2966.2006.10907.x
Smolčić, V., Delvecchio, I., Zamorani, G., et al. 2017, A&A, 602, A2, doi: 10.1051/0004-6361/201630223
Spinoglio, L., Fernández-Ontiveros, J. A., & Malkan, M. A. 2022, ApJ, 941, 46, doi: 10.3847/1538-4357/ac9da2

Spinoglio, L., Fernández-Ontiveros, J. A., & Malkan, M. A. 2024, ApJ, 964, 117, doi: 10.3847/1538-4357/ad23e4

Stalevski, M., Fritz, J., Baes, M., Nakos, T., & Popović, L. Č. 2012, MNRAS, 420, 2756, doi: 10.1111/j.1365-2966.2011.19775.x

Stalevski, M., Ricci, C., Ueda, Y., et al. 2016, MNRAS, 458, 2288, doi: 10.1093/mnras/stw444

Stone, M., Pope, A., McKinney, J., et al. 2022, ApJ, 934, 27, doi: 10.3847/1538-4357/ac778b

Thorne, K. S. 1974, ApJ, 191, 507, doi: 10.1086/152991

Treister, E., Urry, C. M., & Virani, S. 2009, ApJ, 696, 110, doi: 10.1088/0004-637X/696/1/110

Ueda, Y., Akiyama, M., Ohta, K., & Miyaji, T. 2003, ApJ, 598, 886, doi: 10.1086/378940

Uematsu, R., Ueda, Y., Alexander, D. M., et al. 2025, ApJ, 979, 168, doi: 10.3847/1538-4357/ad9f3b

Villa-Vélez, J. A., Buat, V., Theulé, P., Boquien, M., & Burgarella, D. 2021, A&A, 654, A153, doi: 10.1051/0004-6361/202140890

Villani, I., Zappacosta, L., Piconcelli, E., et al. 2026, A&A, 705, A90, doi: 10.1051/0004-6361/202556627

Virtanen, P., Gommers, R., Oliphant, T. E., et al. 2020, Nature Methods, 17, 261, doi: 10.1038/s41592-019-0686-2

Vito, F., Brandt, W. N., Lehmer, B. D., et al. 2020, A&A, 642, A149, doi: 10.1051/0004-6361/202038848

Wu, J., Jun, H. D., Assef, R. J., et al. 2018, ApJ, 852, 96, doi: 10.3847/1538-4357/aa9ff3

Yamada, S., Ueda, Y., Tanimoto, A., et al. 2020, ApJ, 897, 107, doi: 10.3847/1538-4357/ab94b1

Yang, G., Boquien, M., Buat, V., et al. 2020, MNRAS, 491, 740, doi: 10.1093/mnras/stz3001

Yang, G., Caputi, K. I., Papovich, C., et al. 2023, ApJL, 950, L5, doi: 10.3847/2041-8213/acd639

Zhang, B., Zou, F., Brandt, W. N., et al. 2025, ApJ, 978, 9, doi: 10.3847/1538-4357/ad9278

Zhang, Y., Miller, T. B., Price, S. H., et al. 2026, arXiv e-prints, arXiv:2603.00380, doi: 10.48550/arXiv.2603.00380

Zou, F., Brandt, W. N., Gallo, E., Vito, F., & Yu, Z. 2025, ApJ, 990, 94, doi: 10.3847/1538-4357/adf55c